Probing plasmas with ion acoustic waves

Noah Hershkowitz[1] and Young-C Ghim (Kim)

Department of Engineering Physics, University of Wisconsin at Madison, Madison, WI 53706, USA

E-mail: Hershkowitz@engr.wisc.edu

Abstract

Since Langmuir's pioneering studies, low temperature plasma studies have evolved from single positive ion species plasmas, to plasmas with combinations of positive and negative ions in addition to electrons, to plasmas with very heavy negative dust ions. The use of ion acoustic waves, first recognized by Langmuir, as a diagnostic of plasma parameters based on wave frequency, wavelength and phase velocity data in a wide variety of low temperature plasmas, is reviewed. Dispersion relations for all types of unmagnetized plasma are derived as special cases of a single general dispersion relation. Complications associated with grid excitation, such as wave diffraction, excitation of waves at other plasma boundaries and particle burst pseudowaves, are also discussed.

(Some figures in this article are in colour only in the electronic version)

1. Introduction

In 1928, in a paper on oscillations in mercury discharges containing positive ions and electrons, Irving Langmuir introduced the concept of plasmas [1]. In that paper he also reported the presence of low frequency oscillations, inferred the presence of ion acoustic waves, and provided the correct expression for their phase velocity.

In 1929, Lewi Tonks and Irving Langmuir provided details of their experiments on oscillations in plasmas as well as a derivation of the phase velocity of ion acoustic waves associated with the oscillations [2]. They showed that the observed frequencies were consistent with ion acoustic oscillations, but they did not directly observe either standing waves or traveling waves. Their abstract concluded with: 'The correlation between theory and observed oscillations is to be considered tentative until simpler experimental conditions can be attained.' Although the first measurements of standing waves were reported four years later [3], direct observations of traveling waves took quite a while. It was not until 1962 that propagating ion acoustic waves were clearly observed [4]. The measurements were possible because of the evolution of plasma sources and laboratory equipment over the preceding 34 years. It may seem surprising that it took that long. It is not surprising, however, that Langmuir, who had enormous insight into the properties of plasmas, published the correct dispersion

relation for ion acoustic waves in 1928. Plasmas containing both negative and positive ions also support ion acoustic waves, as do dusty plasmas. In all cases, ion acoustic waves have served as diagnostics of electron temperature and ion mass. In two-ion-species plasmas, they provide a measure of the relative concentrations of the ion species. In non-uniform plasmas, they provide drift velocities. As new types of plasmas have been developed and studied, ion acoustic wave phase velocity has continued to be a useful diagnostic technique. This paper reviews their 80 year history.

2. Langmuir started it all

Tonks and Langmuir [2] inferred the presence of ion acoustic waves from frequency measurements of a mercury discharge in an 18 cm diameter spherical glass tube plasma device, shown in figure 1. Energetic primary electrons emitted from 0.025 cm diameter heated tungsten filaments labeled g, c and d, biased with respect to a grounded anode produced the plasma. Immersing an appendix to the tube in a water bath controlled the mercury neutral pressure. Oscillations were detected with a zincite–tellurium crystal detector connected to electrodes mounted on the bulb.

Tonks and Langmuir suggested the presence of high frequency and low frequency non-propagating oscillations and also identified oscillations and waves at frequencies below the ion plasma frequency and above the electron plasma frequency. Their derivation of the ion acoustic wave dispersion relation

---

[1] Noah Hershkowitz is Irving Langmuir Professor of Engineering Physics at the University of Wisconsin at Madison.
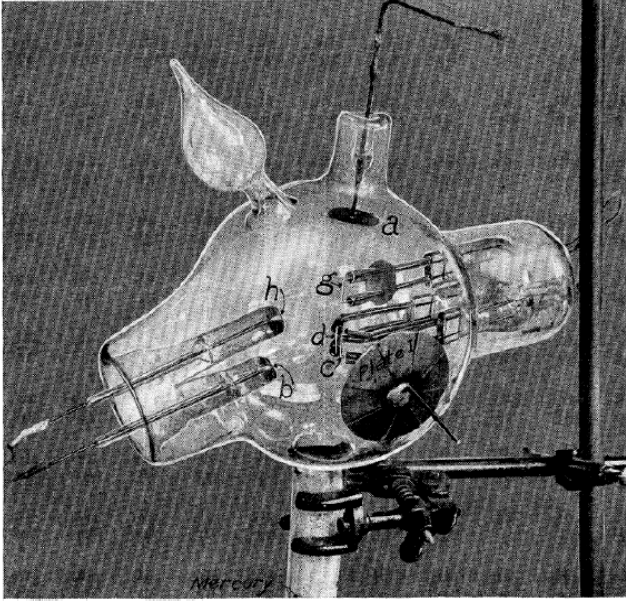
Figure 1. Experimental tube used by Tonks and Langmuir to study plasma oscillations.

Figure 2. Experimental tube used by Revans to study standing waves. Probe P was movable by a magnet.

(using SI units and measuring temperatures in electron volts) follows.

Consider an initially uniform ion distribution and a uniform electron background with a charge density n_e located between two planes perpendicular to the x-axis. If each ion is displaced a small distance ξ that depends on x, the change in ion density is

$$\delta n_i = -n_i \frac{\partial \xi}{\partial x}. \tag{1}$$

Assuming the electron density satisfies the Boltzmann relation

$$n_e = n_{e0} \exp\left(\frac{e\phi}{T_e}\right) \approx n_{e0}\left(1 + \frac{e\phi}{T_e}\right) \tag{2}$$

for small displacements, then

$$\delta n_e \approx n_{e0} \frac{e\phi}{T_e}. \tag{3}$$

Poisson's equation gives

$$\frac{\partial^2 \phi}{\partial x^2} = -\frac{e}{\varepsilon_0}(\delta n_i - \delta n_e) \approx \frac{e}{\varepsilon_0}\left(n_i \frac{\partial \xi}{\partial x} + n_{e0} \frac{e\phi}{T_e}\right). \tag{4}$$

The ion equation of motion is

$$e \frac{\partial \phi}{\partial x} = -m_i \frac{\partial^2 \xi}{\partial t^2}. \tag{5}$$

Equating equations (4) and (5) gives

$$e \frac{\partial^2 \phi}{\partial x^2} = -m_i \frac{\partial}{\partial x}\left(\frac{\partial^2 \xi}{\partial t^2}\right) \approx \frac{ne^2}{\varepsilon_0}\left(\frac{\partial \xi}{\partial x} + \frac{e\phi}{T_e}\right). \tag{6}$$

Taking the derivative of equation (6) with respect to x

$$\frac{\partial^2}{\partial x^2}\left(\frac{\partial^2 \xi}{\partial t^2}\right) + \frac{ne^2}{m_i \varepsilon_0}\left(\frac{\partial^2 \xi}{\partial x^2} + \frac{e}{T_e}\frac{\partial \phi}{\partial x}\right) = 0. \tag{7}$$

Substituting equation (5) gives

$$\frac{\partial^2}{\partial x^2}\left(\frac{\partial^2 \xi}{\partial t^2}\right) + \frac{ne^2}{m_i \varepsilon_0}\left(\frac{\partial^2 \xi}{\partial x^2} - \frac{m_i}{T_e}\frac{\partial^2 \xi}{\partial t^2}\right) = 0. \tag{8}$$

This can be rewritten as

$$\frac{\partial^2}{\partial x^2}\left(\frac{\partial^2 \xi}{\partial t^2} + \frac{ne^2}{m_i \varepsilon_0}\xi\right) - \left(\frac{1}{\lambda_{De}^2}\frac{\partial^2 \xi}{\partial t^2}\right) = 0,$$

$$\frac{\partial^2}{\partial x^2}\left(\frac{\partial^2 \xi}{\partial t^2} + \omega_{pi}^2 \xi\right) - \left(\frac{1}{\lambda_{De}^2}\frac{\partial^2 \xi}{\partial t^2}\right) = 0, \tag{9}$$

where the electron Debye length $\lambda_{De} \equiv \sqrt{\varepsilon_0 T_e/ne^2}$ and the ion plasma frequency $\omega_{pi} \equiv \sqrt{ne^2/\varepsilon_0 m_i}$.

They looked for a solution of the form

$$\xi = \exp\left[i2\pi\left(ft - \frac{x}{\lambda}\right)\right]. \tag{10}$$

This gave

$$f = \left(\frac{\omega_{pi}^2}{(2\pi)^2 + (\lambda^2/\lambda_{De}^2)}\right)^{1/2}. \tag{11}$$

For low frequency long wavelength modes, $\lambda \gg \lambda_{De}$, $2\pi f \ll \omega_{pi}$, they pointed out that the phase velocity was

$$v_\phi = f\lambda \approx \omega_{pi}\lambda_{De} = \sqrt{\frac{T_e}{m_i}} \tag{12}$$

for $\lambda \approx \lambda_{De}$, $\omega \approx \omega_{pi}$.

In 1933, five years after Langmuir's prediction of ion acoustic waves, J J Thomson provided a derivation of ion acoustic waves [5] from ion fluid equations and the Boltzmann
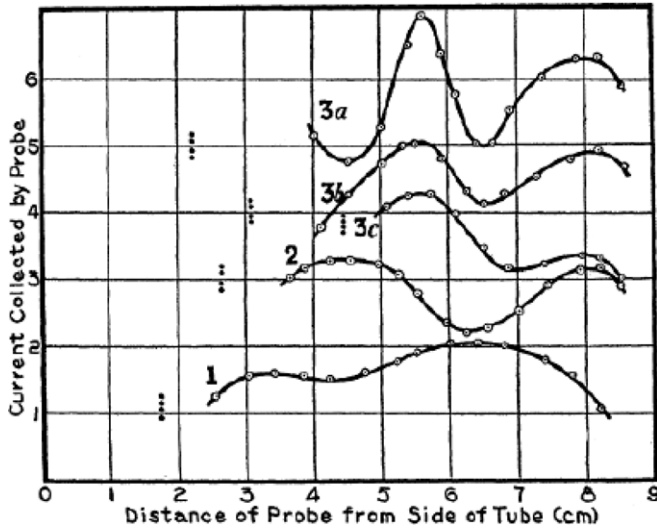
Figure 3. Standing wave profiles observed in Revans' plasma.

relation for electrons. This has been the basis of all fluid derivations of ion acoustic waves ever since. He showed the presence of traveling waves with velocities lying between $\sqrt{T_i/m_i}$ and $\sqrt{(T_i + T_e)/m_i}$.

Later that year, Revans [3] demonstrated the presence of standing waves in a similar discharge device with a spherical bulb, 9 cm in diameter (see figure 2). Spatial profiles of wave intensity along the axis of the device were measured with a Langmuir probe P that was moved with an electromagnet; these are given in figure 3. The current collected by the probe in scans labeled 3a, b, and c showed maxima separated by approximately 2.4 cm, i.e. corresponding to a wavelength of 4.8 cm. This was identified as the octave of the fundamental frequency, i.e. twice the frequency of the fundamental. The measured frequency of the fundamental was approximately 19 kHz, so the corresponding phase velocity of the octave was $1.8 \times 10^5 \, \text{cm s}^{-1}$. This compared favorably with $\sqrt{T_e/m_i} \approx 1.5 \times 10^5 \, \text{cm s}^{-1}$ for the T_e measured by a Langmuir probe of 50 000 to 80 000 °C.

3. Treating plasmas as dielectric materials

The standard derivation of waves in plasmas treats the plasma as a dielectric [6]. The electrostatic wave solutions are found by setting the ε_{zz} component, labeled P in the Stix notation, equal to 0. Starting with the continuity equation, the momentum equation and Poisson's equation, the dispersion relation derived from fluid equations for electrostatic waves in uniform unmagnetized plasmas is given by

$$1 = \sum_j \frac{\omega_{pj}^2}{(\omega - v_{bj}k)^2 - v_{tj}^2 k^2}, \qquad (13)$$

where the sum is over all species including ions and electrons. The plasma frequency of the jth species is $\omega_{pj} = \sqrt{n_j Z_j^2 e^2 / \varepsilon_0 m_j}$, Z_j is the charge, v_{bj} is the drift velocity and the species thermal velocities are v_{tj}. Charge neutrality

requires

$$n_e e + \sum_k Z_{k-} n_{k-} e = \sum_j Z_{j+} n_{j+} e. \qquad (14)$$

The ion acoustic wave solution satisfies $\omega/k \ll v_{te}$, so

$$1 + \frac{\omega_{pe}^2}{v_{te}^2 k^2} \approx \sum_j \frac{\omega_{pj}^2}{(\omega - v_{bj}k)^2 - v_{tj}^2 k^2}. \qquad (15)$$

Equation (15) provides a convenient way to derive the dispersion relation for ion acoustic waves in all the cold plasma systems that have been studied since Langmuir's initial recognition of their existence. In this paper it is used to derive all of the dispersion relations.

The simplest case is no ion beam, one cold positive ion species and no negative ions:

$$1 + \frac{\omega_{pe}^2}{v_{te}^2 k^2} \approx \frac{\omega_{pi}^2}{\omega^2 - v_{ti}^2 k^2}. \qquad (16)$$

Dividing by ω_{pi}^2 gives

$$\frac{1}{\omega_{pi}^2} + \frac{1}{(\gamma_e T_e/m_i)k^2} \approx \frac{1}{\omega^2 - v_{ti}^2 k^2}. \qquad (17)$$

Assuming $\gamma_e = 1$ and $\omega/k \gg v_{ti}$

$$\frac{1}{\omega_{pi}^2} + \frac{1}{(T_e/m_i)k^2} \approx \frac{1}{\omega^2}. \qquad (18)$$

Defining $T_e/m_i = c_s^2$

$$\frac{1}{\omega_{pi}^2} + \frac{1}{c_s^2 k^2} \approx \frac{1}{\omega^2}. \qquad (19)$$

So

$$\omega^2 \approx \frac{\omega_{pi}^2}{1 + (\omega_{pi}^2/c_s^2 k^2)} = \frac{\omega_{pi}^2}{1 + (1/\lambda_{De}^2 k^2)} \qquad (20)$$

in agreement with the expression derived by Tonks and Langmuir. Note that for $\omega \ll \omega_{pi}$, the phase velocity, $\omega/k \approx c_s$, so the phase velocity is equal to the group velocity which is why it is called an acoustic wave.

4. Tone burst measurements detect ion acoustic waves

4.1. In Q machine plasmas

The plasma sources employed by Langmuir and others for over three decades were difficult to study not only because they were very noisy electrically but also because the electronic devices of the time were very primitive. The noise was a consequence of non-uniform plasma generation. The invention and development of the Q machine in the early 1960s changed the experimental landscape by providing a quiet plasma source in which to make measurements. Potassium and cesium plasmas were produced by contact ionization at a W electrode and confined by a 12 kG axial magnetic field. The source provided a 'quiet' low noise plasma with $T_e \approx T_i$.
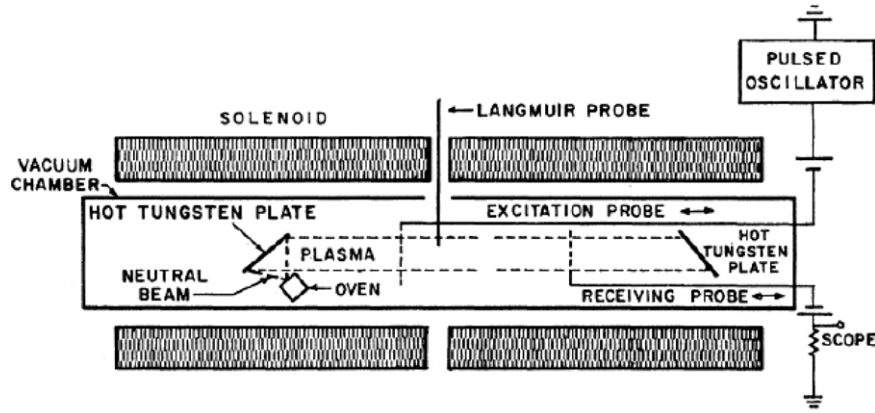
Figure 4. Schematic diagram of the Q machine used to study ion acoustic waves. The hot tungsten plates were separated by 90 cm. The receiving grid is labeled receiving probe.
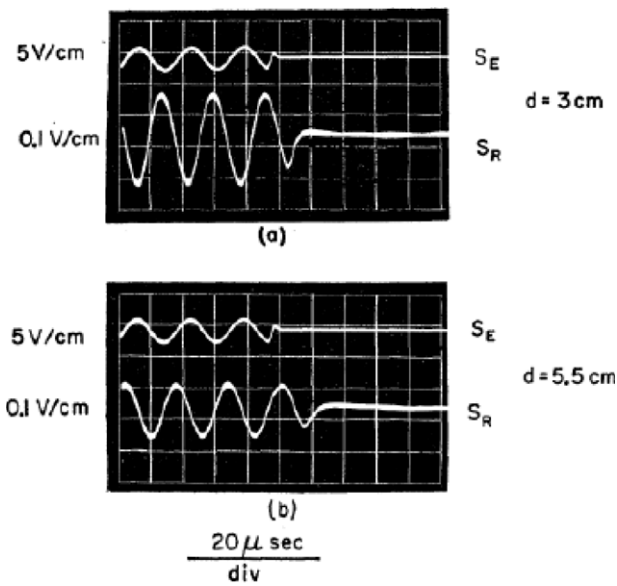
Figure 5. Excitation (S_E) and received signals (S_R) at exciting grid-receiving grid separations of 3 and 5.5 cm. Both time delay and damping are apparent.

Combined with improved electronics, Wong *et al* [4] succeeded in exciting ion acoustic waves by applying low frequency voltage tone bursts to a negatively biased grid in a Q machine in 1962, shown in figure 4 [7]. Strong damping, identified as Landau damping, was observed because $T_e \approx T_i$. The wave phase velocity was reported to be [8]

$$\frac{\omega}{k} = K\sqrt{\frac{T}{m_i}} \qquad (21)$$

with $K = 2$. The origin of the factor of 2 was unknown in that paper.

Data received by a negatively biased grid separated from the launching grid by 3 and 5.5 cm are compared in figure 5. The time shift in the received signal with increasing probe separation is apparent. The experiment was complicated by a steady state plasma drift v_d away from the W source electrode, described in a second paper [7].

The plasma drift resulted in a Doppler shift of the phase velocity so the measured phase velocity

$$v_{\phi\,\mathrm{meas}} = \frac{\omega}{k} \pm v_d \qquad (22)$$

for measurements parallel or anti-parallel to the drift. While this phenomenon complicated the measurement of the phase velocity, it also provided a diagnostic technique of plasma drifts. This paper provided references to kinetic calculations [8, 9] that were consistent with $K = 2$.

4.1.1. The phase velocity for finite temperature. Starting with equation (15)

$$\frac{\omega_{\mathrm{pe}}^2}{(\gamma_e T_e/m_e)k^2} \approx \frac{\omega_{\mathrm{pi}}^2}{\omega^2 - (\gamma_i T_i/m_i)k^2},$$

$$\frac{1}{(\gamma_e T_e/m_i)k^2} \approx \frac{1}{\omega^2 - (\gamma_i T_i/m_i)k^2},$$

$$\left(\frac{\omega}{k}\right)^2 \approx \frac{\gamma_e T_e}{m_i} + \frac{\gamma_i T_i}{m_i}. \qquad (23)$$

The electron and ion thermal velocities can be written $v_{t\,j}^2 = \gamma_j T_j/m_j$ where $j = e$ or i. The ratio of specific heats $\gamma \equiv C_P/C_V$ can be 1 or 3 for collisionless plasma, depending on whether the waves are isothermal or adiabatic, or 5/3 for collisional adiabatic waves [8, 9]. The reason that $K = 2$ can be understood by considering fluid equation results with the choice of $\gamma_e = 1$ and $\gamma_i = 3$. Experiments reported the following year in unmagnetized rare gas plasmas showed that $\gamma_e = 1$ was a good choice in that system. Choosing $\gamma_i = 3$

$$\frac{\omega}{k} \approx \pm\left(1 + \frac{3T_i}{T_e}\right)^{1/2} c_s, \qquad (24)$$

where $c_s \equiv \sqrt{T_e/m_i}$.

Taking $T_e = T_i$

$$\frac{\omega}{k} \approx \pm 2c_s. \qquad (25)$$
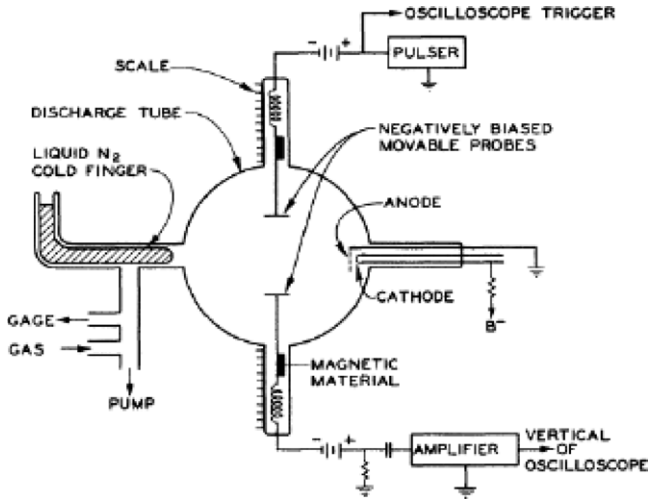
Figure 6. Schematic of apparatus used to detect tone burst in low pressure rare gas plasmas operated at 10^{-3} Torr. The plasma source was a hot tungsten cathode surrounded by a wire cage anode.
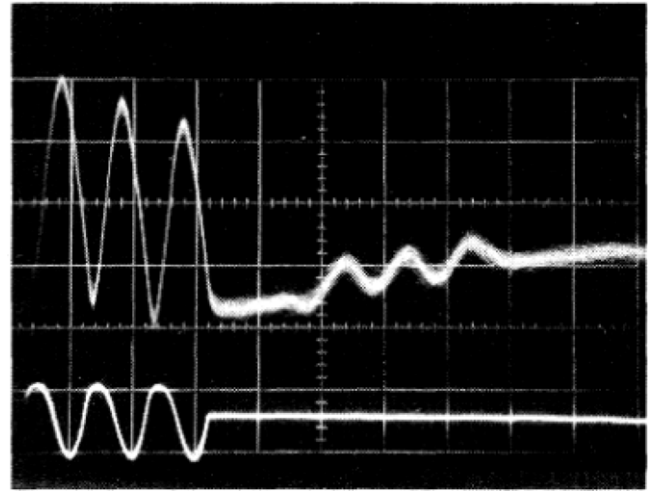
Figure 7. Excitation signal (lower trace) and signal detected by a negatively biased Langmuir probe (upper trace). The time scale was $10\,\mu$s per large division. The upper trace was inverted.

4.1.2. Drift velocity. In the presence of an ion drift v_{di} and a single ion species, equation (15) becomes

$$\frac{\omega_{pe}^2}{v_{te}^2 k^2} \approx \frac{\omega_{pi}^2}{(\omega - v_{di}k)^2 - v_{ti}^2 k^2}, \tag{26}$$

$$\frac{1}{\lambda_{De}^2 k^2} \approx \frac{\omega_{pi}^2}{(\omega - v_{di}k)^2 - v_{ti}^2 k^2},$$

$$\omega - v_{di}k \approx \pm(c_s^2 + v_{ti}^2)^{1/2}k, \tag{27}$$

$$\omega - v_{di}k \approx \pm\left(1 + \frac{\gamma_i T_i}{T_e}\right)^{1/2} c_s k. \tag{28}$$

Assuming $T_i = T_e$ with $\gamma_i = 3$,

$$\frac{\omega}{k} \approx \pm 2c_s + v_{di}. \tag{29}$$

4.2. In rare gas plasmas

In 1965, Alexeff and Jones [10] excited ion waves with sine wave tone bursts to a grid mounted in collisionless rare gas plasmas; see figure 6. They found there were operating parameter spaces with relatively low noise levels. A high pass filter was used to reduce the noise further. Unlike the experiments of Wong *et al* [7], waves were detected with a small movable cylindrical Langmuir probe biased to collect ion saturation current. An example of the detected wave signal is given in figure 7. A signal showing little or no delay, identified as 'an electrostatically coupled signal', was also detected. The wave group velocity, determined from time-of-flight measurements of the detected wave packets, was found to be equal to the pulse group velocity. The waves were found to have Doppler shifts corresponding to drift velocities of at most 10% of the wave velocities, which depended on the location within the discharge chamber.

The results for He, Ne, Ar, Kr, and Xe plasma were summarized in table 1. It is apparent that the value of γ_{exp} best corresponds to 1.0 for all gases and that no apparent contribution comes from T_i because $T_i \ll T_e$.

5. CW measurements also detect ion acoustic waves

Wave excitation with tone bursts does not directly determine either ω or k. Fourier analysis of the tone burst shows a variety of frequency components in the launched signal and that signal damps both in space and in time. An alternative approach is to launch the wave with a CW source and to measure the wave spatial profile with a Langmuir probe. This gives a boundary value problem with real ω and complex k. In 1971, Bernstein *et al* [11] used a double balanced mixer to record 'interferometer traces' of ion waves in a 3 mTorr 90 MHz inductive Ar plasma (see figure 8). They used closely spaced grids, 4.5 cm in diameter with a mesh size of 2.5×10^{-2} cm chosen to be smaller than the Debye length $\lambda_{De} = 3 \times 10^{-2}$ cm. The argon plasma density was 5×10^8 cm^{-3} at a neutral pressure of 3 mTorr.

5.1. Diffraction

It is tempting to analyze interferometer traces in terms of collisional damping or Landau damping. However, interferometer traces of grid launched ion waves often exhibited more complicated phenomena and occasionally showed traces that increased in amplitude with distance from the grid before damping. Bernstein *et al* [11] and Hirshfield *et al* [12] reported good examples of traces showing combinations of growth and damping (see figure 9) and identified this phenomenon as Fresnel diffraction.

Bernstein *et al* showed [11] that the observed wave amplitude pattern resulting from the application of an oscillating charge density to a transparent grid immersed in a low temperature plasma with Boltzmann electrons is

$$\varphi(\vec{r}) = -\int d^3\vec{r'} \frac{\exp(ik|\vec{r} - \vec{r'}|)}{|\vec{r} - \vec{r'}|} \rho(\vec{r'}), \tag{30}$$

where ρ is the charge density at the grid, k is the wavenumber of the launched wave and the integral is over the grid. The

Table 1. Summary of plasma parameters and measured γ_{exp} for rare gases.

Gas	T_e (eV)	$V_{expt.} \times 10^{-5}$ (cm s^{-1})	$\gamma_{expt.}$	$N_e \times 10^{-9}$ (cm^{-3})	$P \times 10^3$ (Torr)	Electron mean-free path (cm)
			Quiescent plasmas			
He	9.63	15.1	0.94	0.38	2.5	20
Ne	0.91	2.05	0.94	3.8	13.0	15
A	0.64	1.26	1.00	2.4	2.8	70
Kr	0.84	0.90	0.81	4.4	2.1	95
Xe	0.79	0.79	1.03	11.0	1.4	140
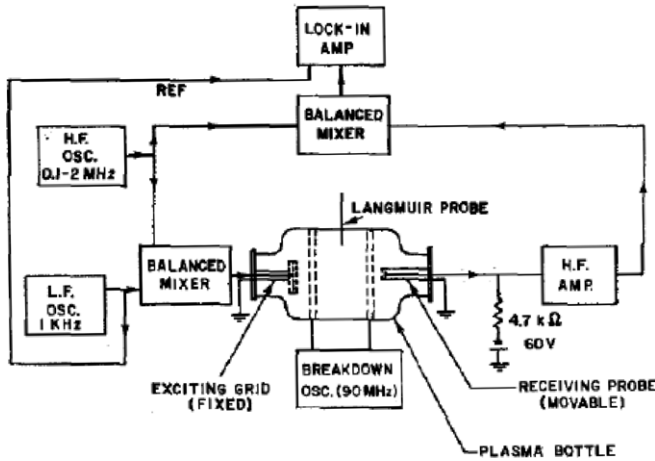
Figure 8. Schematic of apparatus used to detect CW 'interferometer traces' of ion acoustic waves.
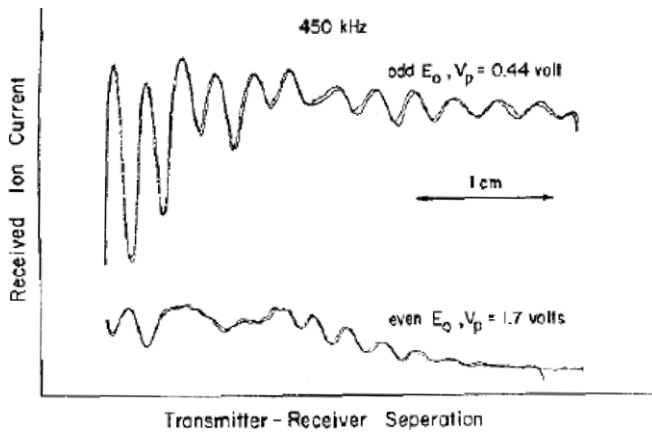
Figure 9. 'Interferometer traces' detected by a negatively biased Langmuir probe. The upper signal corresponded to odd excitation of the two closely spaced grids. The lower signal corresponded to even excitation of the two closely spaced grids.

wave potential along the axis of the grid is

$$\varphi(z) = \varphi_0(\omega)\{\exp[-ik(z^2 + R^2)^{1/2}] - \exp(-ikz)\}, \quad (31)$$

where R is the grid radius.

The key parameter in Fresnel diffraction is the ratio of the wavelength to the grid radius, λ/R. The real part of equation (31) is graphed versus x/λ as a function of λ/R in figure 10, with $\lambda = 2\pi/k$ [13]. The interference pattern is evident out to $z = 2\pi R^2/\lambda$ and then falls off as z^{-1}. For an argon plasma with $T_e = 1$ eV, $c_s = 1.6 \times 10^5$ cm s^{-1} so for
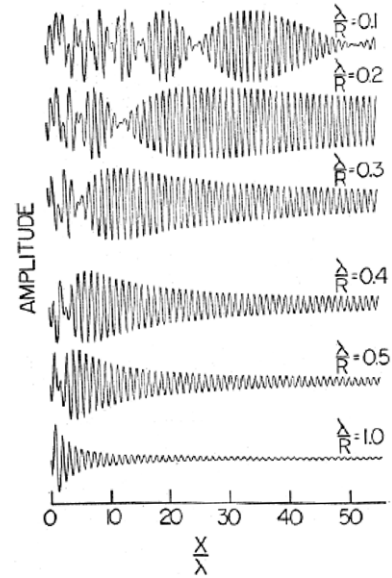
Figure 10. Solutions of equation (31) for several values of λ/R.

100 kHz, λ equals 1.6 cm. For $R = 4$ cm, $\lambda/R = 0.4$ so the interference extends to 63 cm, i.e. $x/\lambda = 40$.

5.2. Multi-dipole chamber

Further studies of diffraction took advantage of a major improvement in low temperature plasma sources. In 1973, Limpaecher and Mackenzie [14] found a new way to produce quiet plasma. They surrounded unmagnetized plasma with a multi-dipole magnetic field created by permanent magnets with alternating polarities facing the plasma. Electrons emitted from filaments mounted inside the device as shown in figure 11 were accelerated across virtual anodes concentric with the filaments and effectively confined by the multi-dipole field resulting in a background of isotropic homogeneous primary electrons. This resulted in very uniform, very quiet plasmas with density perturbations $(\delta n/n) \approx 3 \times 10^{-4}$. Nonuniformity over the volume 31 cm diameter by 69 cm length were less than 1%. Grid launched waves shown in figure 12 with density perturbations $\delta n/n = 5 \times 10^{-3}$ could be observed without filtering.

5.3. More diffraction

Experiments carried out in a multi-dipole plasma device by Christensen and Hershkowitz [13] with a 14 cm radius grid
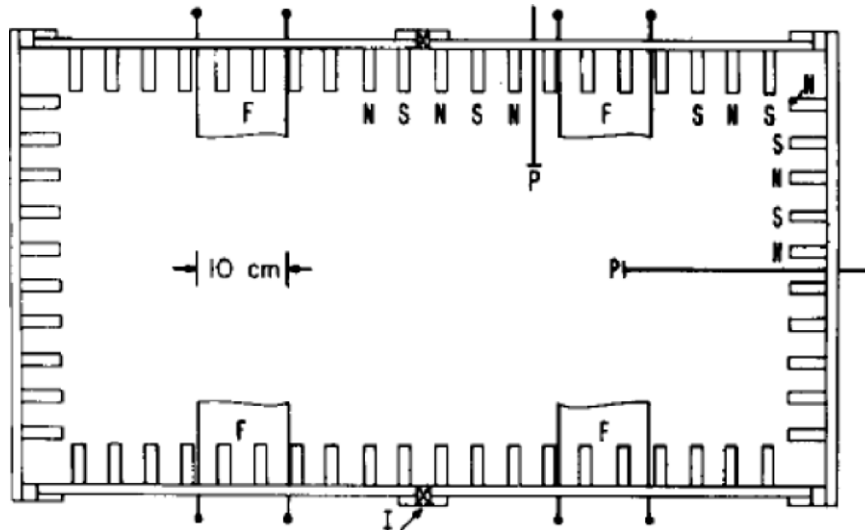
Figure 11. Schematic description of cylindrical multi-dipole device.
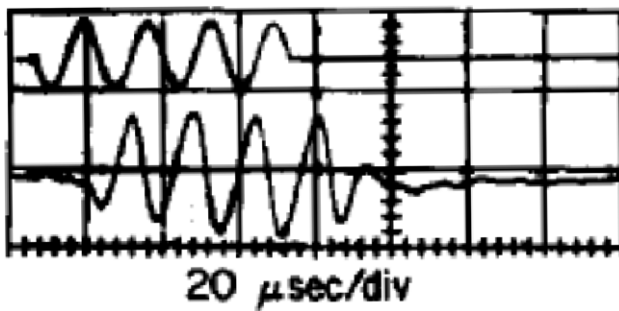
Figure 12. The upper trace is the signal applied to a negatively biased grid (0.5 V, 60 kHz). The lower trace is the signal detected ion saturation current with $\delta n/n = 5 \times 10^{-3}$.

used a time filtered technique to generate interferometer traces. The results shown in figure 13 give wave amplitude versus position from the grid as a function of frequency ranging from 30 to 85 kHz corresponding to λ/R ranging from 0.7 to 0.3. These results are similar to those shown in figure 10 and to those reported by Hirshfield *et al* [11, 12].

6. Signal applied to grids excite ion acoustic waves at all plasma boundaries

Probe measurements on the axis of the cylindrical multi-dipole device also demonstrated that ion acoustic waves were excited simultaneously with those excited at the grid at all plasma boundaries [15]. Plane waves propagating toward the grid were excited at the planar end-walls as seen in figure 14. Cylindrical waves propagated radially inward with collisional damping competing with geometric growth. On-axis probe data at two different positions show a pulse (identified by the arrow) that arrives at a delay time equal to R_c/c_s where R_c is the chamber radius (see figure 15). It appears that the waves were excited by time varying changes in the global plasma potential associated with the modulated current drawn to the grid. The changes in plasma potential at the grounded boundaries acted the same as a fluctuating potential to a conductor bounding a uniform
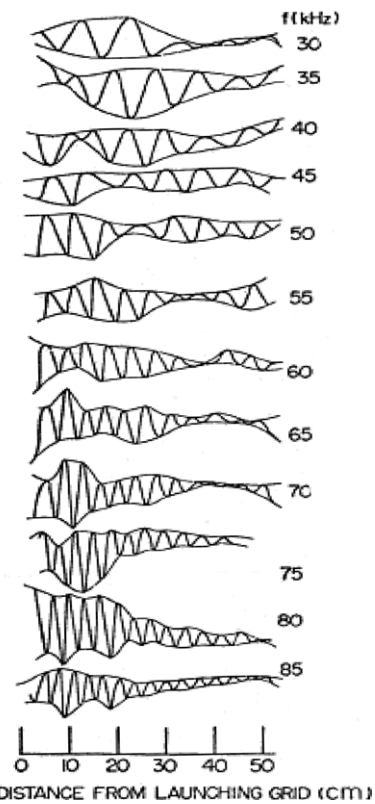
Figure 13. 'Interferometer traces' detected by a positively biased Langmuir probe. Solid lines are drawn to indicate the envelope.

plasma. The experiments were carried out at neutral pressure of 1.5×10^{-5} Torr with a base pressure of 3×10^{-7} Torr so charge exchange and impurities were not significant.

7. Pseudowaves

Application of a tone burst to a grid in a plasma can launch more than waves. If the amplitude of the excitation voltage is much greater than T_e/e, it was found that particle bursts could
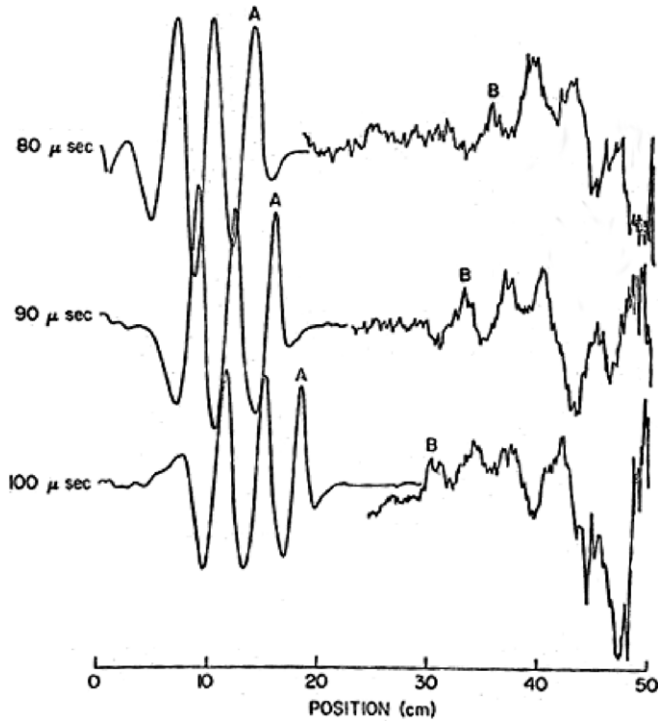
Figure 14. Waves launched by the grid (A) and launched by the end-wall (B) are graphed versus position at 80, 90 and 100 μs after signal application. Signal B is amplified by a factor of 10 compared with signal A.
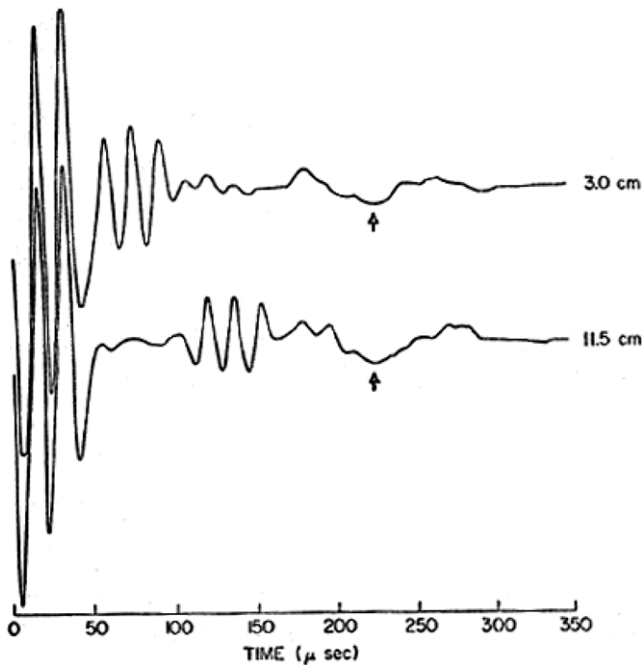
Figure 15. Probe signal versus time detected at 3 and 11.5 cm from the launching grid.

be launched [16]. The signal detected by a negatively biased probe resembled a wave signal (see figure 16) and was named a pseudowave. The data in figure 16 also show that a weak ion acoustic wave was simultaneously excited by the voltage pulse in a xenon plasma.
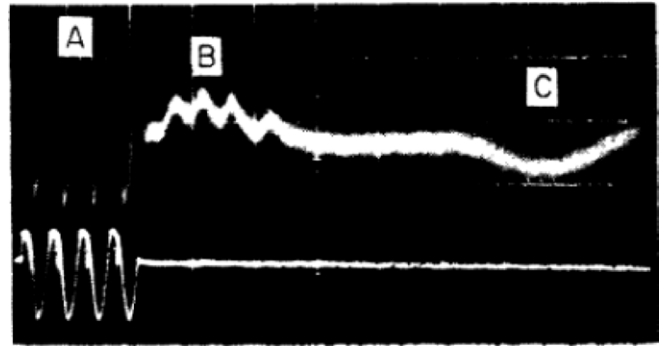
Figure 16. The lower trace shows an approximately 200 kHz 4 cycle tone burst exciting signal that was applied to the excitation grid. The upper trace shows the direct coupled signal (A), the pseudowave (B), and the ion acoustic wave (C) detected by a Langmuir probe 7.5 cm from the grid.
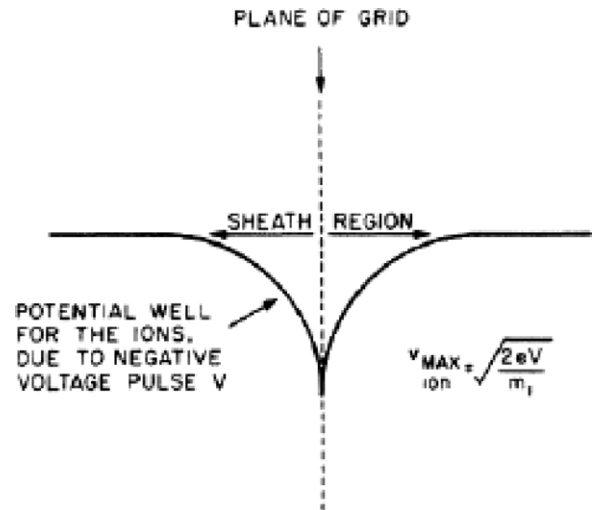
Figure 17. Schematic of the plasma potential profile near the grid.

The transit time of the pseudowave was found to be equal to

$$t = \frac{L}{\sqrt{(2eV/m_i)}}, \tag{32}$$

where V is the amplitude of the applied voltage tone burst. It was argued that ions accelerated to the grid in a potential well created by the application of the large amplitude tone burst retained their full energy if the negative potential was quickly removed; see figure 17.

The tone burst consisted of four cycles of a 500 kHz wave with a period of 5 μs. The tone burst frequency was chosen to be just above the ion plasma frequency. This is a consequence of ion transit time across the plasma sheath near the launching grid. Sobolewski *et al* [17] have shown that the ion transit time of a dc sheath can be written as

$$\tau = 2 \left(\frac{mV}{2e} \right)^{1/4} \left(\frac{\varepsilon_0}{J_0} \right)^{1/2}, \tag{33}$$
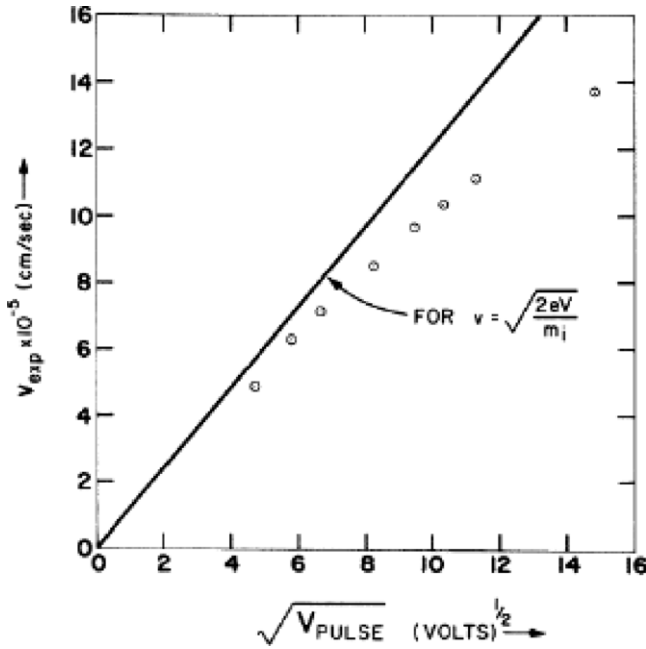
Figure 18. Pseudowave velocity versus square root of exciting voltage amplitude.

where J_0 is the ion current density at the sheath edge. Assuming J_0 is equal to the Bohm current density $n_i e \sqrt{(T_e/m_i)}$.

$$\tau = 2 \left(\frac{m_i V}{2e} \right)^{1/4} \left(\frac{\varepsilon_0}{n_i e \sqrt{(T_e/m_i)}} \right)^{1/2}$$

$$= 2 \left(\frac{eV}{2T_e} \right)^{1/4} \left(\frac{\varepsilon_0 m_i}{n_i e^2} \right)^{1/2} \approx 1.7 \left(\frac{eV}{T_e} \right)^{1/4} \frac{1}{\omega_{pi}}. \quad (34)$$

The pseudowave velocity and hence the transit time was also found to be increased as the applied voltage amplitude was increased as shown in figure 18.

Ion acoustic waves should not be excited for $\omega > \omega_{pi}$ so why were ion acoustic waves excited by the tone burst? Examination of the detected signal in figure 16 shows that only a lower frequency Fourier component, lower than ω_{pi}, was excited.

8. What is the relative ion concentration in two positive ion species plasmas?

It is tempting to guess that the relative ion concentrations of two ion species are equal to the neutral partial pressure ratios. Direct measurement is possible using mass spectrometers with ionizers turned off, but corrections are needed for losses to extracting apertures and sensitivity to different masses. The phase velocity of ion acoustic waves provides a simple alternative.

Consider low temperature, low pressure plasmas with $T_e \approx 1\,\text{eV}$, $T_i \approx 0.025\,\text{eV}$, $n_e \approx 10^8$–$10^{10}\,\text{cm}^{-3}$ operating at mTorr neutral pressures. Similar plasmas are often employed in basic plasma studies that serve as models of ideal collisionless plasmas and of plasmas employed in semiconductor plasma processing. Since $T_e \gg T_i$, taking
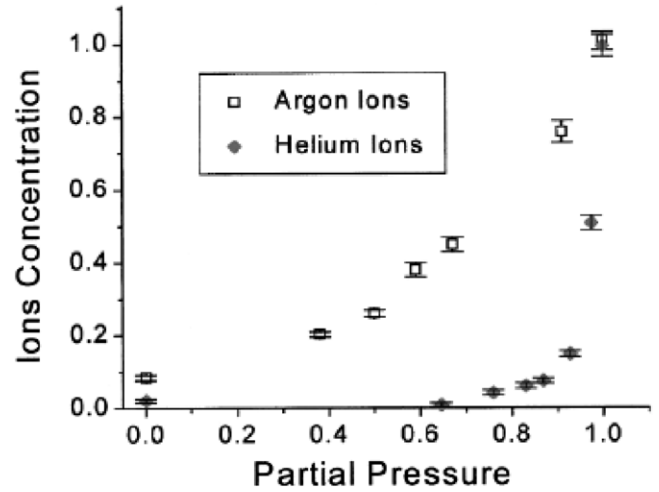
Figure 19. Ion concentrations in Ar/Xe and He/Xe plasmas as a function of Ar and He partial pressures.

$P = 0$ (equation (13)) for the long wavelength dispersion relation in non-drifting two ion species plasma gives

$$\frac{\omega_{pe}^2}{v_{te}^2 k^2} \approx \frac{\omega_{p1}^2}{\omega^2} + \frac{\omega_{p2}^2}{\omega^2}. \quad (35)$$

The ion acoustic phase velocity is

$$\frac{\omega^2}{k^2} \approx \frac{n_1 T_e}{n_e m_1} + \frac{n_2 T_e}{n_e m_2} = \frac{n_1 c_{s1}^2}{n_e} + \frac{n_2 c_{s2}^2}{n_e},$$

$$\frac{\omega^2}{k^2} = \frac{n_1 c_{s1}^2}{n_e} + \frac{(n_e - n_1)c_{s2}^2}{n_e} = \frac{n_1 c_{s1}^2}{n_e} + \left(1 - \frac{n_1}{n_e} \right) c_{s2}^2 \quad (36)$$

so the phase velocity directly gives n_1/n_e. Representative measurements of the relative concentrations of He$^+$ and Ar$^+$ ions as a function of their partial pressures in a Xe plasma are given in figure 19 [18]. Electron temperature was determined with a Langmuir probe to be 0.5–3 eV, the density $10^{10}\,\text{cm}^{-3}$ and the pressure ranged from 1 to 20 mTorr.

Note that a partial pressure of 90% of He corresponds to an ion density of only 10%. This diagnostic technique shows that using the fractional neutral density as an estimate of the fractional ion density is not a good approach. Unfortunately, phase velocity does not provide enough information to determine the relative ion concentrations when three or more ion species are present.

9. Determining relative concentrations in negative ion–positive ion plasmas

Negative ion–positive ion plasmas are another example of two-ion-species plasmas for which ion acoustic waves can provide ion number density ratios. Starting with $P = 0$ (equation (13)),

$$1 = \sum_j \frac{\omega_{pj}^2}{\omega^2 - v_{tj}^2 k^2}. \quad (37)$$

9

For plasma with one positive ion species with density n_+ and one negative ion species with density n_-

$$1 = \frac{\omega_{pe}^2}{\omega^2 - v_{te}^2 k^2} + \frac{\omega_{p+}^2}{\omega^2 - v_{t+}^2 k^2} + \frac{\omega_{p-}^2}{\omega^2 - v_{t-}^2 k^2}. \quad (38)$$

Assuming $\omega^2 \ll v_{te}^2 k^2$ and quasi-neutrality $n_+ = n_- + n_e$,

$$1 \approx -\frac{((n_+ - n_-)e^2)/\varepsilon_0 m_e}{v_{te}^2 k^2} + \frac{n_+ e^2/\varepsilon_0 m_+}{\omega^2 - v_{t+}^2 k^2} + \frac{n_- e^2/\varepsilon_0 m_-}{\omega^2 - v_{t-}^2 k^2}. \quad (39)$$

Defining $\varepsilon = n_-/n_+$ and $M = m_-/m_+$,

$$\frac{1 - \varepsilon}{c_s^2 k^2} \approx \frac{1}{\omega^2 - v_{t+}^2 k^2} + \frac{\varepsilon/M}{\omega^2 - v_{t-}^2 k^2} - \frac{\varepsilon_0 m_+}{n_+ e^2}. \quad (40)$$

9.1. Plasmas with cold ions

If v_{t+}^2 and v_{t-}^2 are much less than ω^2/k^2, then

$$\frac{\omega^2}{k^2} \approx c_s^2 \frac{1}{(1 + k^2 \lambda_{De}^2)} \frac{1 + (\varepsilon/M)}{1 - \varepsilon}, \quad (41)$$

where

$$\frac{1}{\lambda_{De}^2} = \frac{n_e e^2}{\varepsilon_0 T_e} = \frac{n_i e^2}{\varepsilon_0 m_+} \frac{m_+}{T_e} \frac{n_e}{n_i} = \frac{\omega_{p+}^2}{c_s^2}(1 - \varepsilon).$$

This agrees with the dispersion relation given by Cooney *et al* [19] to describe Ar$^+$ and F$^-$ in Ar/SF$_6$ plasmas.

9.2. Plasmas with finite temperature ions

If we assume following St-Onge *et al* [20] that $v_{t+} = v_{t-} = v_t$ and that $v_t^2 = 3T_+/m_+ = 3T_-/m_-$.

$$\frac{\omega^2}{k^2} \approx c_s^2 \frac{1}{(1 + k^2 \lambda_{De}^2)} \frac{1 + (\varepsilon/M)}{1 - \varepsilon} + 3\tau, \quad (42)$$

where $\tau = T_+/T_e$.

It is important to recognize that the assumption of equal thermal velocities for positive ion and negative ion species is unlikely to apply to many real situations. So equation (42) should be used with care.

St-Onge *et al* used equation (42) to determine relative ion concentrations in a Ar/SF$_6$ plasma in which ion species were not identified. They claimed 'qualitative agreement' with photodetachment measurements as shown in figure 20.

9.3. Negative ion concentration measurements in general

In general, measurements of negative ion to positive ion concentration using ion acoustic waves have agreed qualitatively with measurements made using other techniques such as laser-induced photodetachment (LIPD) and Langmuir probe methods, but have not agreed quantitatively. The problem does not appear to be in the wave measurement.

Amemiya asserted that the negative ion temperature can be determined by taking the second derivative of the probe characteristics [21]. In addition, he stated that the ratio of
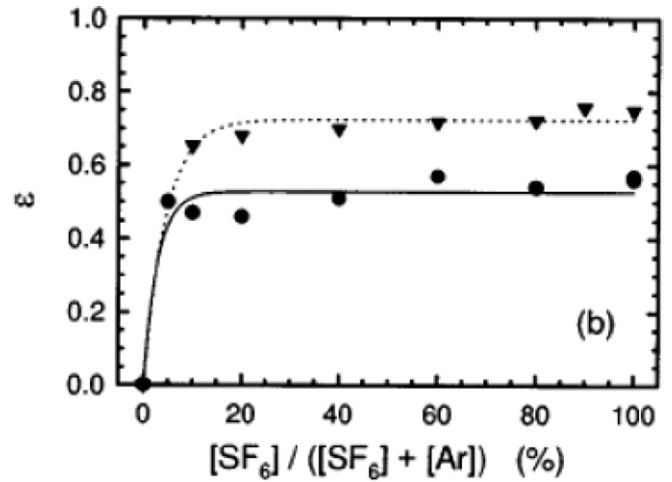
Figure 20. Ratio of negative ion to positive ion density as a function of SF$_6$ partial pressure in Ar/SF$_6$ plasmas measured by ion acoustic wave phase velocity (circles) and LIPD (triangles). ε is defined as n_-/n_+.

saturation current above the plasma potential to ion saturation current gave the negative ion concentration if masses and temperatures of various species in plasmas were known by assuming the negative ions followed Boltzmann relation [21]. However, such an assumption must be used with care because the steady state solution of negative ion momentum equation is not Boltzmann if the equation includes non-linear terms such as the ionization rate and recombination rates.

Shindo *et al* claimed that negative ion concentration could be found in electronegative plasmas by taking the ratio of the ion saturation–electron saturation current ratio in electronegative plasmas to that in a reference electropositive plasmas [22]. Shindo *et al* gives

$$\varepsilon = \frac{n_-(X)}{n_+(X)} = 1 - \frac{i_+(Ar)}{i_+(X)} \frac{i_{es}(X)}{i_{es}(Ar)} \sqrt{\frac{m_+(Ar)}{m_+(X)}} \Omega(X), \quad (43)$$

where i_+, i_{es}, n_- and n_+ denote ion saturation current, electron saturation current, negative ion density and positive ion density in the bulk, respectively. Here, Ar and X denote that pure argon is used as a reference electropositive plasmas and X gas for electronegative plasmas. $m_+(Ar)$ and $m_+(X)$ represent positive ion mass of argon and reduce mass of positive ions for X gas. $\Omega(X)$ stands for the sheath factor of X gas plasmas given by

$$\Omega(X) = \sqrt{2\left(\frac{T_+(X)}{T_e(X)} + \frac{eV_B(X)}{T_e(X)}\right)}$$
$$\times \left[(1 - \varepsilon)\exp\left(-\frac{eV_B(X)}{T_e(X)}\right) - \varepsilon \exp\left(-\frac{eV_B(X)}{T_-(X)}\right)\right], \quad (44)$$

where $V_B(X)$ is a potential drop required from the bulk to the sheath edge to provide positive ions a Bohm speed in electronegative plasmas. Equation (43) is derived by using

10

following relations with quasi-neutrality by Shindo *et al*:

$$i_+(\text{Ar}) \propto n_+(\text{Ar})S\sqrt{\frac{T_e(\text{Ar})}{m_i(\text{Ar})}}, \qquad (45a)$$

$$i_+(X) \propto n_+(X)S\Omega(X)\sqrt{\frac{T_e(X)}{m_i(X)}}, \qquad (45b)$$

$$i_{es}(\text{Ar}) \propto n_e(\text{Ar})S\sqrt{\frac{T_e(\text{Ar})}{m_e(\text{Ar})}}, \qquad (45c)$$

$$i_{es}(X) \propto n_e(X)S\sqrt{\frac{T_e(X)}{m_e(X)}}, \qquad (45d)$$

where S is the planar probe surface area.

However, equation (43) is incorrect since equation (45a) does not include the sheath factor for pure argon plasmas, $\Omega(\text{Ar}) = \exp(-(eV_B(\text{Ar})/T_e(\text{Ar})))$, which corrects the positive ion number density at the sheath edge to that of in the bulk. This is a necessary factor to have logical consistency. $\Omega(X)$ corrects a Bohm speed based on energy conservation assuming collisionless plasmas [23, 24]. It also corrects the number density at the sheath edge by assuming Boltzmann relations for both electrons and negative ions. This does not provide a correct value of ε in the bulk because it is not constant from the bulk to the sheath edge, assuming both negative ions and electron satisfy Boltzmann relations with $T_e \neq T_-$. Even if the Boltzmann relation for negative ions is valid, the value of ε is not the measurement of the ratio in the bulk. Nevertheless, equation (43) has been cited by many researchers [25–27], and $\Omega(X)$ has been assumed to be unity for simplicity in their papers.

Defining a new sheath factor as

$$\Omega(X, \text{Ar}) = \frac{\Omega(X)}{\Omega(\text{Ar})}, \qquad (46)$$

and replacing this new sheath factor with the old sheath factor, $\Omega(X)$, at the end of equation (43) gives the correct expression to find the value of ε at the sheath edge provided that the plasma is collisionless and negative ions and electrons follow Boltzmann relations. Thus, quantitative disagreement between Langmuir probe data using equation (43) and other techniques such as laser Thomson scattering [26] and ion acoustic wave phase velocity measurements [22] is expected because these techniques find the value of ε in the bulk.

To further explore this question, we produced a weakly collisional electronegative plasmas in a dc multi-dipole chamber [28] with 0.35 mTorr Ar and 0.05 mTorr O_2. Neutral gases were ionized by energetic electrons emitted from hot thoriated tungsten filaments biased at -60 V with respect to the chamber wall, and the discharge current was set to be 0.6 A. Langmuir probe data showed that the effective electron temperature in the bulk was 1.05 ± 0.05 eV which corresponded to the Ar sound speed of 1600 ± 40 m s^{-1} by assuming that there was a negligible amount of oxygen positive ions. It also found that electron number density was 1.7×10^9 cm^{-3} in the bulk. The ion acoustic wave phase velocity measurement was
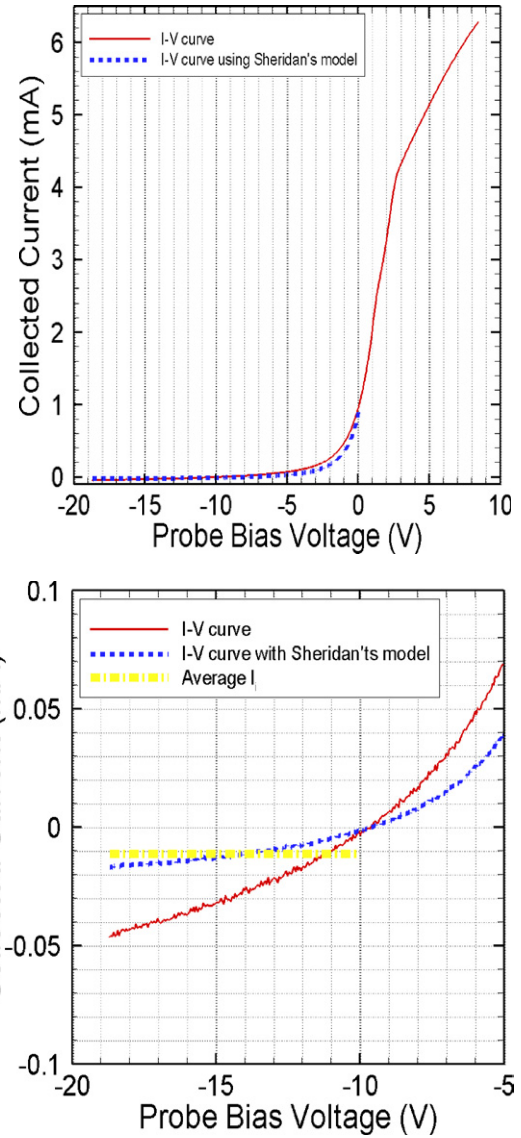
Figure 21. (*a*) The Langmuir probe trace in Ar/O$_2$ plasmas in bulk plasma with Sheridan's model correction on ion saturation current. (*b*) Magnified Langmuir probe trace of ion saturation current compared with Sheridan's model.

carried out and yielded 2000 ± 30 m s^{-1} which corresponded to the value of 0.14 for $\varepsilon = n_-/n_+$ using equation (41). Quasi-neutrality requires that the positive ion number density should be 1.9×10^9 cm^{-3} in the bulk.

If we assume that there is a double layer potential structure [29] so that negative ions do not exist at the sheath edge, then the drift velocity of positive ions is the usual Bohm speed, $(T_e/m_i)^{1/2}$ and positive ions follow the Boltzmann relation. With the probe surface area of 63.3 mm^2, an emissive probe measurement of $V_B = 1.0$ V, and the ion drift velocity to the probe of 1600 m s^{-1}, ion saturation current is calculated to be 11.3 μA. The ion saturation current with Sheridan's model correction on the probe characteristics [30] was 10.7 ± 0.5 μA; see figure 21.

Analysis of theoretical and experimental ion saturation current data suggests the existence of double layer potential structures in electronegative plasmas with small fractions of

negative ions. Experiments are needed to provide direct measurement of the double layer potential structures.

10. Dusty plasmas

10.1. Dust acoustic waves with cold dust

Writing $P = 0$ (equation (13)) in the low frequency limit, inclusion of massively negative charged cold dust and assuming no ion drifts gives

$$1 \approx \frac{\omega_{\text{pe}}^2}{-v_{\text{te}}^2 k^2} + \frac{\omega_{\text{pD}}^2}{\omega^2} + \frac{\omega_{\text{p+}}^2}{\omega^2 - v_{\text{t+}}^2 k^2}, \quad (47)$$

where $\omega_{\text{pD}}^2 = n_{\text{D}} e^2 Z_{\text{D}}^2 / \varepsilon_0 m_{\text{D}}$ is the dust plasma frequency and for simplicity is assumed that each dust particle has the same radius and charge Ze.

Rao *et al* assumed [31] a hot background positive ion plasma in equilibrium with cold negatively ionized dust so that $\omega^2 \ll v_{\text{t+}}^2 k^2$, and charge neutrality gives

$$n_{\text{e}} + Z_{\text{D}} n_{\text{D}} = n_+,$$

$$1 \approx -\frac{n_{\text{e}} e^2 / \varepsilon_0 m_{\text{e}}}{v_{\text{te}}^2 k^2} - \frac{n_+ e^2 / \varepsilon_0 m_+}{v_{\text{t+}}^2 k^2} + \frac{((n_+ - n_{\text{e}}) Z_{\text{D}} e^2) / \varepsilon_0 m_{\text{D}}}{\omega^2}. \quad (48)$$

Rearranging and defining $\delta \equiv n_+ / n_{\text{e}}$

$$\frac{\varepsilon_0 m_+}{n_+ e^2} \approx -\frac{1}{(T_{\text{e}}/m_+) k^2 \delta} - \frac{1}{(T_+/m_+) k^2} + \frac{Z_{\text{D}}(1 - (1/\delta))(m_+/m_{\text{D}})}{\omega^2} \quad (49)$$

so

$$\omega^2 \approx \frac{c_{\text{s,dust}}^2 k^2 Z_{\text{D}}(\delta - 1)}{\lambda_{\text{De}}^2 k^2 + 1 + \eta \delta}$$

$$= \frac{c_{\text{s,dust}}^2 k^2 (Z_{\text{D}}(\delta - 1)/(1 + \eta \delta))}{(k^2 \lambda_{\text{De}}^2/(1 + \eta \delta)) + 1} \omega^2$$

$$= \beta^2 c_{\text{s,dust}}^2 k^2 \left[1 + \frac{k^2 \lambda_{\text{De}}^2}{1 + \eta \delta} \right]^{-1}, \quad (50)$$

$c_{\text{s,dust}} \equiv \sqrt{T_{\text{e}}/m_{\text{D}}}$, $\eta \equiv T_{\text{e}}/T_+$ $\beta^2 \equiv Z_{\text{D}}(\delta - 1)/(1 + \eta \delta)$ and λ_{De} is the electron Debye length.

10.2. High frequency dust acoustic waves—hot dust

Most of the studies of dust acoustic waves have concentrated on the low frequency behavior. The dust ions are very heavy so the low frequencies are the order of 100 Hz. Recently, Thomas *et al* [32] have studied the 'high frequency' dust acoustic waves. A dc glow discharge was produced in their dusty plasma device by biasing a 2.5 cm diameter anode at 350–400 V in an argon neutral pressure of 100–200 mTorr. The dust was kaolin powder with a nominal diameter of $\sim 1\,\mu$m. Waves were excited by sinusoidal modulation to the anode discharge current. Their results in figure 22 show that the wavenumber is proportional to the applied frequency for small frequencies. However, above a certain frequency ($\omega > 280$ rad s^{-1}), the dominant wavenumber did not change perceptibly (circles). Careful examination of the data found fine structure for which the wavenumbers did increase with frequencies (squares). In
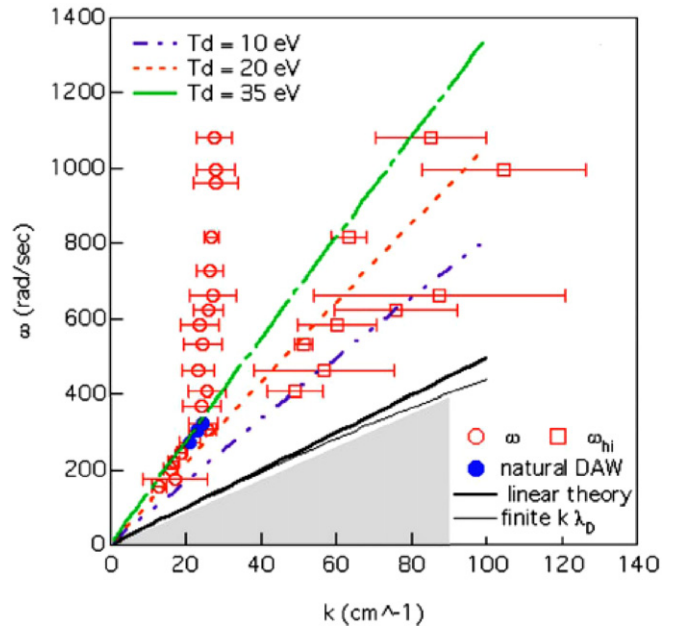
Figure 22. Comparison of calculated and measured dispersion relations in dusty plasmas.

this figure, the solid line corresponds to theoretical predictions with temperature of the dust particles, T_{D}, about 1/40 eV and assumed dust particle average radius of $0.5\,\mu$m. The thin solid line corrects the linear theory by including the expected Debye length. These two lines contain disagreement with the measured values. Using larger values of the dust radius makes the lines fall into gray-shaded region which increases the discrepancy. Thomas *et al* [32] suggested that agreement could be attained by using hot temperatures of dust particles, $T_{\text{D}} \approx 10$, 20 and 35 eV.

The dispersion relation for 'hot' dust particles for which the phase velocity of dust acoustic waves was much less than the thermal velocity of the dust so $\omega^2 \ll k^2 v_{\text{te}}^2$, and $\omega^2 \ll k^2 v_{\text{t+}}^2$ follows from

$$1 \approx -\frac{\omega_{\text{pe}}^2}{k^2 v_{\text{te}}^2} - \frac{\omega_{\text{p+}}^2}{k^2 v_{\text{t+}}^2} + \frac{\omega_{\text{pD}}^2}{\omega^2 - k^2 v_{\text{tD}}^2}. \quad (51)$$

Rearranging equation (51) gives

$$\frac{\omega_{\text{pD}}^2}{\omega^2 - k^2 v_{\text{tD}}^2} \approx 1 + \frac{\omega_{\text{pe}}^2}{k^2 v_{\text{te}}^2} + \frac{\omega_{\text{p+}}^2}{k^2 v_{\text{t+}}^2},$$

$$\omega^2 - k^2 v_{\text{tD}}^2 \approx \frac{k^2 \omega_{\text{pD}}^2}{k^2 + (1/\lambda_{\text{De}}^2) + (1/\lambda_{\text{D+}}^2)}, \quad (52)$$

where $1/\lambda_{\text{D}j}^2 = \omega_{\text{p}j}^2 / v_{\text{t}j}^2$ for jth species.

Defining

$$\frac{1}{\lambda_{\text{D}}^2} = \frac{1}{\lambda_{\text{De}}^2} + \frac{1}{\lambda_{\text{Di}}^2},$$

$$\omega^2 - k^2 v_{\text{tD}}^2 \approx \frac{k^2 \omega_{\text{pD}}^2}{k^2 + (1/\lambda_{\text{D}}^2)},$$

$$\omega^2 \approx k^2 v_{\text{tD}}^2 + \frac{k^2 c_{\text{s,dust}}^2}{1 + k^2 \lambda_{\text{D}}^2}, \quad (53)$$

where $c_{\text{s,dust}}^2 = \omega_{\text{pD}}^2 \lambda_{\text{D}}^2$.
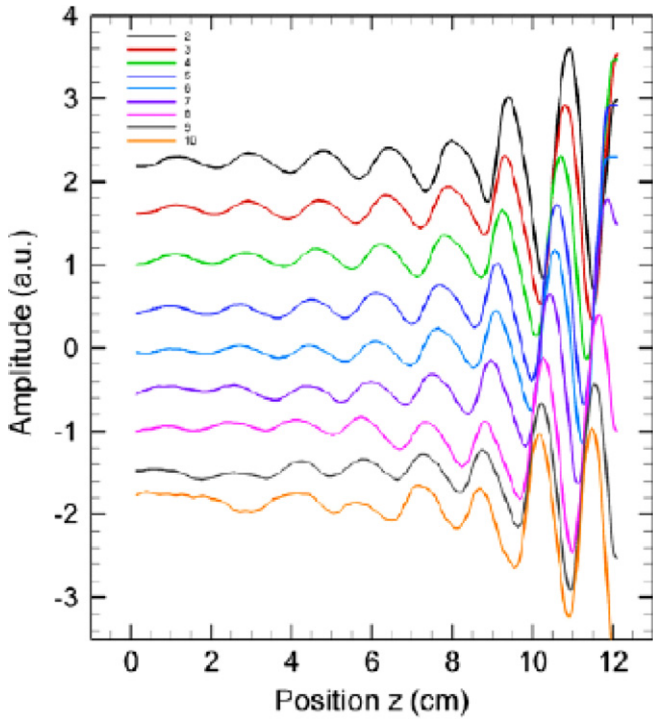
Figure 23. Interferometer traces near a biased plate in a 0.5 mTorr Ar/0.2 mTorr Xe plasma corresponding to delay times ranging from 2 to 10 μs.

In the long wavelength limit, the phase velocity is

$$\frac{\omega}{k} \approx \sqrt{v_{tD}^2 + c_{s,dust}^2}. \tag{54}$$

Measurement of the low frequency phase velocity can be used to determine v_{tD}. It is apparent in figure 22. that dust temperatures in the range of 10–35 eV are required to describe the measured data.

11. Presheath–sheath measurements—non-uniform drifts

Sometimes the contribution of the ion drift velocity to the ion acoustic wave phase velocity is a problem in need of a solution. Examples include the original Q machine ion acoustic wave experiments of Wong *et al* [7] and the wave measurements of St-Onge *et al* [20]. Sometimes the drift is the phenomenon that matters. This is the case in studies of ion motion in the presheath that accelerates ions to the Bohm velocity at the sheath–presheath boundary.

Oksuz *et al* [33] showed that the phase velocity near the sheath–presheath boundary in weakly collisional Ar/Xe plasmas was approximately twice the phase velocity in the bulk plasma. As shown in figures 23 and 24 the ion acoustic wave phase velocity in the bulk region was measured to be $830 \pm 80 \, \mathrm{m\,s^{-1}}$ (at $z = 15$ cm), whereas the velocity at the sheath–presheath boundary was $1820 \pm 100 \, \mathrm{m\,s^{-1}}$ (at $z = 0.6$ cm). This gave the ion drift velocity of $990 \pm 140 \, \mathrm{m\,s^{-1}}$ in agreement with the phase velocity in the bulk region within the experimental error. Ion acoustic wave phase velocity data in the bulk provided the relative concentrations [18] of Ar and Xe
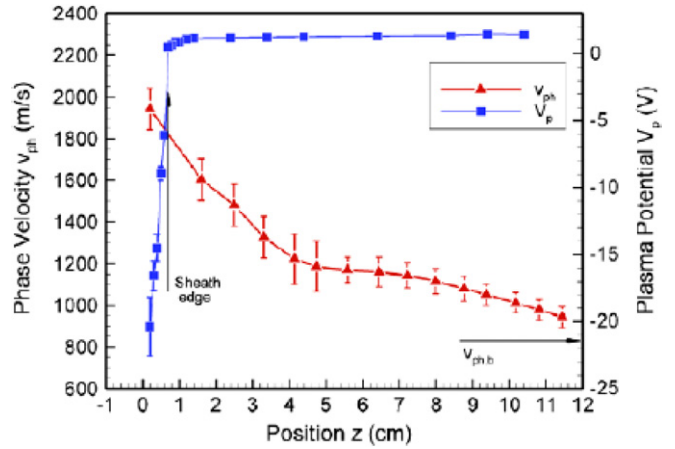
Figure 24. Plasma potential profile determined from emissive probe data and the ion acoustic wave phase velocity profile based on data in figure 23.

ions. Data in the argon/xenon plasma also showed that the ion acoustic wave phase velocity was approximately twice the bulk phase velocity. These results mean that the ion drift velocities at the sheath–presheath boundary are equal to the ion acoustic wave velocity in the bulk plasma. The two species result also agreed with laser-induced fluorescence measurements of the Xe and Ar drift velocities [34].

12. Conclusions

Ion acoustic wave frequency, wavelength and phase velocity data have been the basis of valuable plasma diagnostics since Langmuir first described ion acoustic waves in 1928. Early plasma sources had significant spatial anisotropy resulting high electronic noise levels. With the evolution of quieter plasma sources and much better electronics, both temporal behavior and spatial behavior have become much easier to determine. Mercury discharges were replaced with rare gas discharge in similar glass discharge tubes and then by multi-dipole discharge devices. The first clear observation of propagating ion acoustic waves was made in a Q machine in Cs$^+$ and K$^+$ plasmas with $T_e = T_i$ in the presence of significant damping and then in rare gas plasmas with $T_e \gg T_i$ resulting in much less damping. Multi-dipole devices then provided extremely quiet plasmas. Over the years, phase and group velocity have become increasingly easier to measure. Low temperature plasma studies have evolved from single positive ion species plasmas, to plasmas with combinations of positive and negative ions in addition to electrons, to plasmas with very heavy negative dust ions.

Here we have shown that the dispersion relation for all types of ion acoustic waves can be derived as special cases of a single general dispersion relation. With it we can equally describe ion acoustic waves in positive ion plasmas, negative ion plasmas, dusty plasmas, plasmas with beams, and all combinations of hot and cold ions. We argue that ion acoustic wave phase velocity is a better diagnostic of the ratio of negative ion to positive ion density than Langmuir probe data.

In single species plasmas with cold ions of known mass, ion acoustic wave phase velocity provides the electron

temperature T_e. If T_e is available from Langmuir probe data, it provides the ion mass. If ions are drifting, phase velocity data can be used to provide the drift velocity, e.g. near a negatively biased boundary. If two ion plasmas species are present, it provides the relative ion concentrations for plasmas with two positive ions or one positive and one negative ion.

Ion acoustic waves are usually launched by grids and this can lead to complications such as wave diffraction, excitation of waves at other plasma boundaries, and particle burst pseudowaves.

As new combinations of plasmas are created, it is likely that ion acoustic waves will continue to lead the way in providing valuable data.

Acknowledgment

References

[1] Langmuir I 1928 *Proc. Natl Acad. Sci.* **14** 627
[2] Tonks L and Langmuir I 1929 *Phys. Rev.* **33** 195
[3] Revans R W 1933 *Phys. Rev.* **44** 798
[4] Wong A Y, D'Angelo N and Motley R W 1962 *Phys. Rev. Lett.* **9** 415
[5] Thomson J J and Thomson G P 1933 *Conduction of Electricity through Gases*, Part II (Cambridge: Cambridge University Press) p 353
[6] Stix T H 1992 *Waves in Plasmas* (New York: Springer)
[7] Wong A Y, Motley R W and D'Angelo N 1964 *Phys. Rev.* **133** A436
[8] Fried B D and Gould R W 1961 *Phys. Fluids* **4** 139
[9] Spitzer L Jr 1962 *Physics of Fully Ionized Gases* 2nd edn (New York: Interscience) p 55
[10] Alexeff I and Jones W D 1965 *Phys. Rev. Lett.* **15** 286
[11] Bernstein I B, Hirshfield J L and Jacob J H 1971 *Phys. Fluids* **14** 628
[12] Hirshfield J L, Jacob J H and Baldwin D E 1971 *Phys. Fluids* **14** 615
[13] Christensen T and Hershkowitz N 1977 *Phys. Fluids* **20** 840
[14] Limpaecher R and MacKenzie K R 1973 *Rev. Sci. Instrum.* **44** 726
[15] Christensen T and Hershkowitz N 1977 *Phys. Lett.* A **61** 170
[16] Alexeff I, Jones W D and Lonngren K 1968 *Phys. Rev. Lett.* **21** 878
[17] Sobolewski M A, Olthoff J K and Wang Y 1999 *J. Appl. Phys.* **85** 3966
[18] Hala A M and Hershkowitz N 2001 *Rev. Sci. Instrum.* **72** 2279
[19] Cooney J L, Aossey D W, Williams J E, Gavin M T, Kim H S, Hsu Y-C, Scheller A and Lonngren K E 1993 *Plasma Sources Sci. Technol.* **2** 73
[20] St-Onge L, Margot J and Chaker M 1998 *Appl. Phys. Lett.* **72** 290
[21] Amemiya H 1990 *J. Phys. D: Appl. Phys.* **23** 999
[22] Shindo M, Uchino S, Ichiki R, Yoshimura S and Kawai Y 2001 *Rev. Sci. Instrum.* **72** 2288
[23] Oksuz L and Hershkowitz N 2005 *Plasma Sources Sci. Technol.* **14** 201
[24] Oksuz L and Hershkowitz N 2004 *Plasma Sources Sci. Technol* **13** 263
[25] Boruah D, Pal A R, Bailung H and Chutia J 2003 *J. Phys. D: Appl. Phys.* **36** 645
[26] Noguchi M, Hirao T, Shindo M, Sakurauchi K, Yamagata Y, Uchino K, Kawai Y and Muraoka K 2003 *Plasma Sources Sci. Technol* **12** 403
[27] You S J, Kim S S and Chang H Y 2005 *Phys. Plasmas* **12** 083502
[28] Lee D, Severn G, Oksuz L and Hershkowitz N 2006 *J. Phys. D: Appl. Phys.* **39** 5230
[29] Lieberman M A and Lichtenberg A J 2005 *Principles of Plasma Discharges and Materials Processing* 2nd edn (New York: Wiley) p 340
[30] Sheridan T E 2000 *Phys. Plasmas* **7** 3084
[31] Rao N N, Shukla P K and Yu M Y 1990 *Planet. Space Sci.* **38** 543
[32] Thomas E Jr, Fisher R and Merlino R L 2007 *Phys. Plasmas* **14** 123701
[33] Oksuz L, Lee D and Hershkowitz N 2008 *Plasma Sources Sci. Technol.* **17** 015012
[34] Lee D, Hershkowitz N and Severn G D 2007 *Appl. Phys. Lett.* **91** 041505